Assessment of Separation and Agglomeration Tendency of Non-metallic Inclusions in an Electromagnetically Stirred Aluminum Melt

Cong Li, Thien Dang, Mertol Gökelma, Sebastian Zimmermann, Jonas Mitterecker, and Bernd Friedrich

Abstract

Presence of non-metallic inclusions (NMIs) reduces surface quality and mechanical properties of aluminum products. The development of good NMIs removal practices relies on the understanding of inclusion behaviors with respect to separation and agglomeration particularly in the turbulent flow. In the scenario of electromagnetically induced recirculated turbulent flow, the concerned behaviors of inclusions with different sizes have rarely been investigated experimentally. In the presented study funded by AMAP Open Innovation Research Cluster, reference materials were prepared with uniformly distributed NMIs (SiC and $MgAl_2O_4$) via an ultrasound-involved casting route. Reference materials were charged into an aluminum melt where turbulent flow was promoted via electromagnetic force. Microscopical analysis shows non-significant agglomeration tendency of SiC, $MgAl_2O_4$, and TiB_2 inclusion. Time-weight filtration curve, PoDFA, and Spark Spectrometer results suggest a strong dependence of separation rate on particle size. Analytical models were established to estimate the collision rate of particles and to evaluate separation probability of different sized particles.

C. Li (✉) · B. Friedrich
IME Process Metallurgy and Metal Recycling, RWTH Aachen University, 52056 Aachen, Germany
e-mail: cli@ime-aachen.de

T. Dang
TRIMET Aluminium SE, 45356 Essen, Germany

M. Gökelma
Department of Materials Science and Engineering, Izmir Institute of Technology, 35430 Izmir, Turkey

S. Zimmermann · J. Mitterecker
Former student of IME Process Metallurgy and Metal Recycling, RWTH Aachen University, 52056 Aachen, Germany

Keywords

Non-metallic inclusions • Melt cleanliness • Separation • Agglomeration

Introduction and Motivation

During primary and secondary aluminum production, non-metallic Inclusions (NMIs) are formed during smelting, re-melting, and melt handling processes. Without proper NMIs removal process, NMIs pose difficulties in subsequent metal working processes and dramatically deteriorate the surface quality and mechanical property of aluminum products [1].

Conventional NMIs removal processes namely sedimentation, salt fluxing, gas purging, and filtration have been well established in productions [2]. The concept of improving the conventional NMIs removal process based on forced agglomeration of the particle was proposed firstly by Szekely [3]. The author suggested that intensive mixing can promote the coagulation of particles and bigger particles can be easily removed by either floatation or filtration. In simulation works, SiC particles and Al_2O_3 particles were also reported to have a tendency to form agglomerates in the aluminum melt [4, 5]. Marechal et al. [6] reported agglomeration trend of Al_2O_3 and SiC particles with aluminum melt in laminar flow conditions. Nevertheless a robust way to evaluate the size evolution during particle agglomeration was missing. So far the experimental investigation of NMI particles agglomeration behavior in turbulent flow conditions is rare to find. Not to mention the study of agglomeration behavior of practical inclusions namely $MgAl_2O_4$ which is frequently found in 5xxx alloys. The reasons lie mainly in difficulties of introduction of inclusions into the melt and dispersing them homogeneously. Commercial metal matrix composite (MMC) offers a simple way to introduce of NMIs. For instance using Duralcan® MMC, particles like SiC, Al_2O_3 can be readily introduced into the melt. Nevertheless

S. Broek (ed.), *Light Metals 2023*, The Minerals, Metals & Materials Series,
https://doi.org/10.1007/978-3-031-22532-1_120

particles in the commercial MMC are often clustered to a different extent and type of particles cannot be customized to meet specific interests.

Electromagnetic (EM) separation, as a relative new separation process, has been proposed since decades yet the application of such process on removal of NMIs from aluminum melt remains in lab-scale [7]. Theoretical [8, 9] works including simulation ones have demonstrated the fundamental principle of EM separation. Meanwhile a simulation work is performed in the heavy metal melt predicted particle size-dependent separation rate [10]. With respect to aluminum melt, several trials demonstrated the effectiveness of EM separation [11]. Nevertheless, to the best knowledge of authors, no trials havre been performed on examining separating rate difference of NMIs with different sizes during EM separation treatment.

In the presented study funded by Advanced Metals and Process (AMAP) Open Innovation Research Cluster, we firstly developed process routes capable of fabricating reference materials with customized inclusion type and meanwhile well-dispersed inclusions. SiC, $MgAl_2O_4$, and TiB_2 particles were charged into the melt via either reference materials or master alloy to represent practical carbide, oxide, and boride inclusions present in 5xxx aluminum alloy. An electromagnetically driven melt was employed to provide intensive stirring conditions for agglomeration study. The treated melt were evaluated via metallography, time-weight filtration curve, PoDFA, and Spark Spectrometer analysis. In the meantime, a separation study was conducted in two different scale furnaces to clarify the size dependent separation rate of particles in the electromagnetically driven flow. Analytical models were established to help interpret experimental findings.

Experimental Methodology

Reference Materials Preparation

Two types of reference materials were fabricated in order to ensure a controlled way for introducing artificial inclusions with a defined concentration as well as particle size distribution.

1st type of reference material A356-SiC was fabricated by diluting Duralcan® Metal Matrix Composite (MMC) which contains ca. 30 vol% SiC particles. The dilution was made under a protective atmosphere in a pre-cleaned parent A356 melt with assistance of a rotor. The melt was mixed for certain time upon charging of MMC and afterwards a final casting was performed to obtain reference materials. 2nd Type of reference material namely 5xxx-$MgAl_2O_4$ was obtained by a combination of stir-casting and ultrasound melt treatment. $MgAl_2O_4$ powders were charged onto the surface of a commercial pure aluminum melt which was agitated via a rotor under a protective atmosphere. Afterwards the melt with suspended particles were casted into a steel mould. The upper part of the obtained ingot enriched with $MgAl_2O_4$ particles (incl. clusters) and pores were sectioned and charged into another prepared 5xxx parent melt. Ultrasound melt treatment was performed for the 5xxx-$MgAl_2O_4$ melt for the sake of degassing and simultaneously break up the big clusters. Treated melt was casted to obtain reference materials (weighing 1–2 kg). Both type of reference materials were sectioned into small pieces for further characterization and usage.

Separation and Agglomeration Trials

The investigation of particle separation and agglomeration was performed using two vacuum induction furnaces (VIF) in difference scales. Table 1 lists dimension, and electromagnetic (EM) parameter of the two used induction furnaces.

For 0.1 L VIF, the set-up snapshot and schematic of the melting facility is shown in Fig. 1. The trials started by first of all preparing base melt (5083 alloy). Afterwards inclusions (SiC, $MgAl_2O_4$) were introduced via the reference materials. Upon charging, the furnace was powered on to generate EM stirring for 60 s. When stirring was completed, the melt along with steel crucible was taken out of the coil and quenched in the water tank.

The trial procedure in 1 L VIF is given in Fig. 2. 5083 alloy was used to prepare the base melt. The main difference comparing with 0.1 L VIF trials is the integration of a melt cleaning step (Fig. 2b). Reference material

Table 1 Dimension, electromagnetic parameter of vacuum induction furnaces (VIF)

Name	0.1 L vacuum induction furnaces	1 L vacuum induction furnaces
Height of crucible (net value, m)	0.065	0.19
Diameter of crucible (net value, m)	0.04	0.11
Frequency (kHz)	10	4
Number of inductor turns-N_c	6.75	5
Length of coil (m)-l_c	0.146	0.081
Inductor current (A)-I_c	540	1423

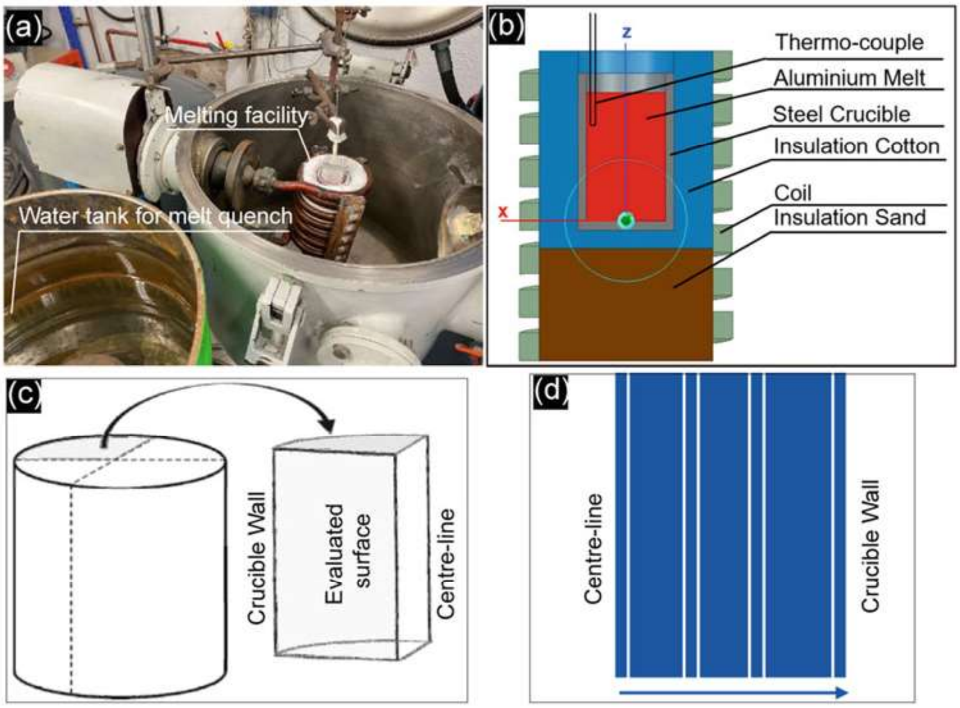

Fig. 1 0.1 L vacuum induction furnace trial procedures: **a** set-up snapshot; **b** schematic of heating facility; **c** sectioning; **d** assessed columns, blue arrow marked radial direction

Fig. 2 Procedure of 1 L vacuum induction furnace trial. EM stands for electromagnetic

A356-SiC and master alloy Al-5Ti-1B in the coil form were used in 1 L VIF trials (Fig. 2c, d). Evaluation of inclusions were conducted for melts in non-stirred status and electromagnetically stirred status. Trial parameters for both 0.1 L VIF and 1 L VIF scenarios are listed in Table 2.

Inclusions Evaluation

The quenched ingots from 0.1 L VIF trial were sectioned and subject to metallographic preparation, as is shown schematically in Fig. 1c. Upon metallograpic preparation of the sample surface, particle spatial distribution and size distribution were assessed and compared with that of the reference materials. Figure 1d shows schematically the evaluation region of the sample in a white column. Optical Micrographs (OMs) were transformed from RGB into binary graphs using Matlab®. The same software was used to quantify particles with respect to area fraction and size distribution within each view field.

The filtration process through a PoDFA set-up was recorded in real-time videos. In each of the 12 trials, the melt was at the same temperature before transferring into the PoDFA crucible and the vacuum level generated beneath the

Table 2 Parameter of trials and evaluation methods

Vacuum induction furnace (L)	Trial Nr.	Inclusion	Conc.	EMS* time (s)	Evaluation method
0.1	1	SiC	0.1 wt %	60	Metallography
	2	$MgAl_2O_4$	0.1 wt %	60	
1	3, 4, 5	SiC	25 ppm	0	Metallography (inc. PoDFA) filtration-curve SS**
	6, 7, 8	SiC	25 ppm	60	
	9, 10, 11	TiB_2	39 ppm	0	
	12, 13, 14	TiB_2	39 ppm	60	

* EMS stands for electromagnetic stirring
** SS stands for spark spectrometer

filter disc during filtration was the same. The data concerning the filtrated mass value (kg) as a function of time (s) was extracted and plotted into time-weight filtration curve. Solidified PoDFA samples containing the filter and possibly the filtration cake were sectioned and prepared metallographically. Afterwards OMs were taken to evaluate the collected inclusions. Spark Spectrometer (SS) analysis were performed for samples taken right before PoDFA filtration.

Results

Characterization of Reference Materials

Figure 3A shows Particle Size Distribution (PSD) of both commercial metal matrix composite (MMC) and A356-SiC reference materials. Note that the normalized particle number fraction within each size sub-range (e.g., 35–40 µm) is represented by a single data point. The graph suggests that with our dilution process, particles were well dispersed. Meanwhile big clusters were broken up with an average particle size reduced from 16.6 to 12.1 µm.

Figure 3b shows PSD of the 5xxx-$MgAl_2O_4$ reference material. The graph demonstrates the effectiveness of the developed process route, i.e., a combination of stir-casting and ultrasound melt treatment. $MgAl_2O_4$ particles were well dispersed with an average size of 21.8 µm.

Agglomeration Behavior of Particles

Agglomeration trials were mainly performed in a 0.1 L vacuum induction furnace (VIF). For SiC particles, normalized particle area fraction for each sub-group of size (e.g., 35–40 µm) was plotted as a function of the particle size (Fig. 4a). The comparison between the sample obtained from 60 s electromagnetically stirred melt and A356-SiC reference material suggest no evidence of agglomeration. On the contrary, a few big clusters seem to be broken up, leading to a shift of particle size to a smaller range and a minor decrease of average of particle diameter. A similar trend of de-agglomeration of particles were observed for the case of $MgAl_2O_4$ (Fig. 4b).

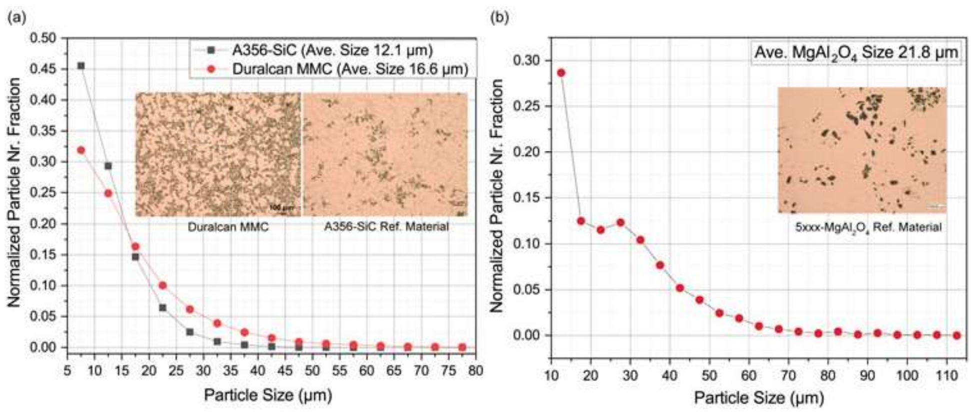

Fig. 3 Particle size distribution in reference materials: **a** A356-SiC; **b** 5xxx-$MgAl_2O_4$. Quantitative results each from at least 40 view fields. Inserts are example optical micrographs

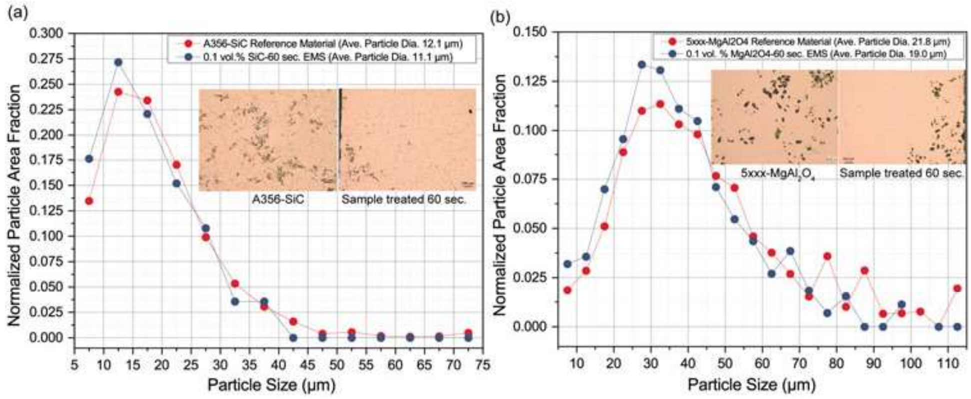

Fig. 4 Normalized particle area fraction within each sub-range of particle size: **a** SiC; **b** $MgAl_2O_4$. Quantitative results of A356-SiC and 5xxx-$MgAl_2O_4$ each from 160 view fields. Inserts are example optical micrographs

Separation Behavior of Particles

In the 0.1 L VIF scenario, the separation of SiC and $MgAl_2O_4$ particles in the near-wall region is shown in Fig. 5. The normalized area fraction of each column (Fig. 1d) for either SiC or $MgAl_2O_4$ particle is plotted as a function of radial distance to the center line. The result shown in Fig. 5 suggests that more $MgAl_2O_4$ (19 μm) were separated than SiC (11 μm) particles under the same EM parameter.

In the 1 L VIF scenario, the separation of SiC particles was evaluated via time-weight filtration curve and PoDFA metallography. Figure 6a gives the time-weight filtration curve of the melt after 0 s EMS and 60 s EMS for SiC particle trials. A noticeably higher filtration rate can be observed for the melt after 60 s stirring. PoDFA metallographic result shown in Fig. 7 suggests a nearly 100 vol% reduction of SiC in the melt. This offers a reasonable explanation for the increased filtration rate shown in Fig. 6a.

In 1 L VIF scenario, the separation of TiB_2 particles was evaluated via time-weight filtration curve, PoDFA metallography, and Spark Spectrometer (SS) analysis. Figure 6b gives the time-weight filtration curve of the melt after 0 s EMS and 60 s EMS for TiB_2 particle trials. Unlike SiC particles, the two curves coincide with each other very well. If one assumes the filtration curve is sensitive primarily to inclusions amount and secondarily to inclusion size distribution, the filtration curve of TiB_2 particles does not suggest

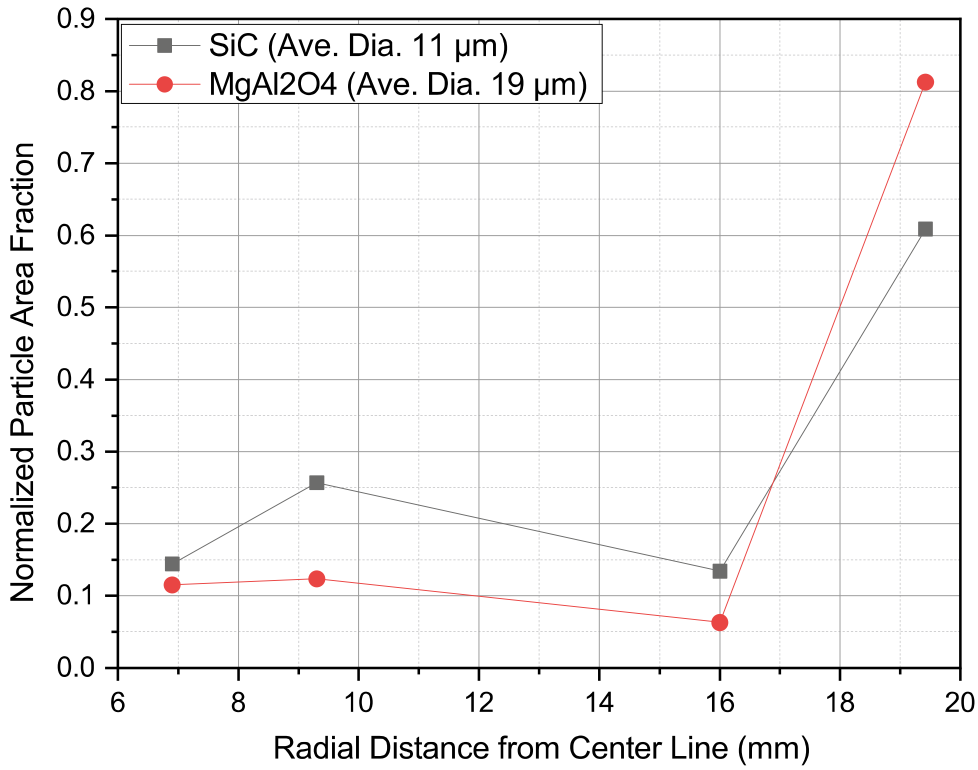

Fig. 5 Normalized particle (SiC and $MgAl_2O_4$) area fraction in radial direction

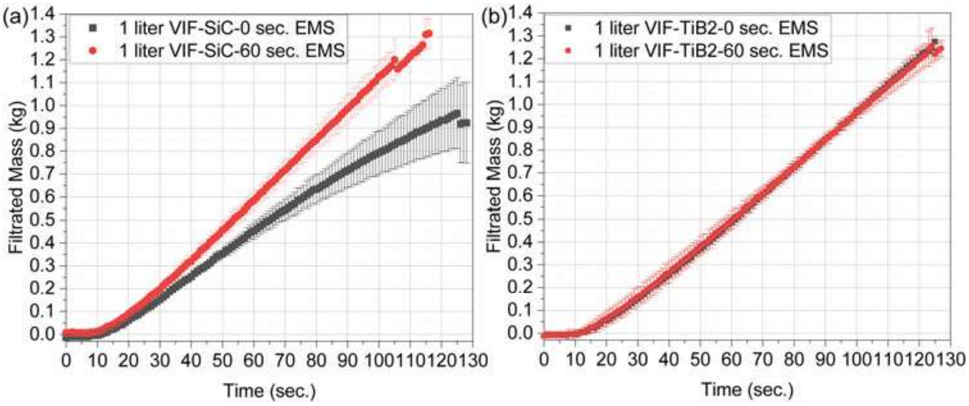

Fig. 6 Time-weight filtration curve from melt after 0 and 60 s electromagnetically stirring (EMS). **a** SiC particle, from trials Nr. 3–8; **b** TiB_2 particle from trial Nr. 9–14. All trials conducted in 1 L vacuum induction furnace (VIF)

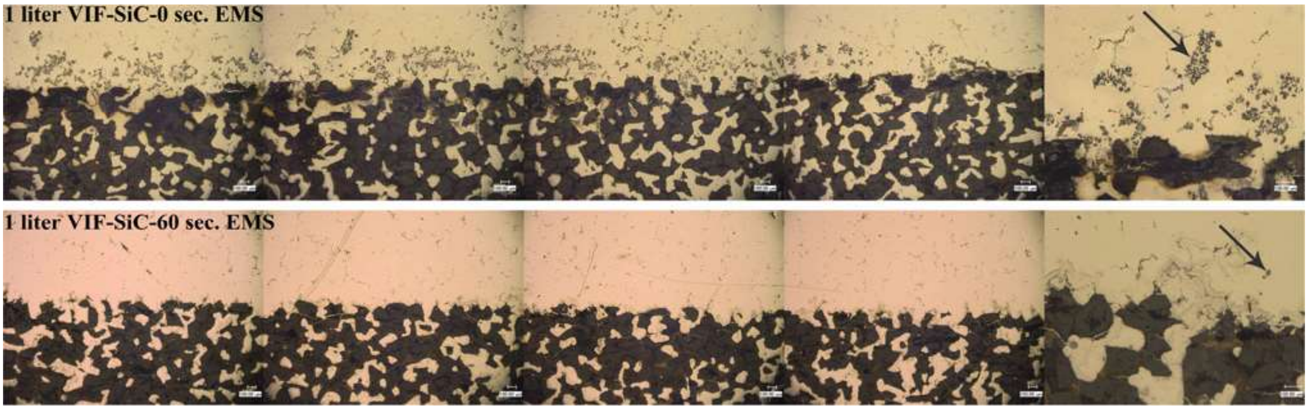

Fig. 7 Micrographs of PoDFA filter (cake) from melt after 0 and 60 s electromagnetically stirring (EMS). Arrows marked SiC particles. Results from trial Nr. 3 and 6 conducted in 1 L vacuum induction furnace (VIF)

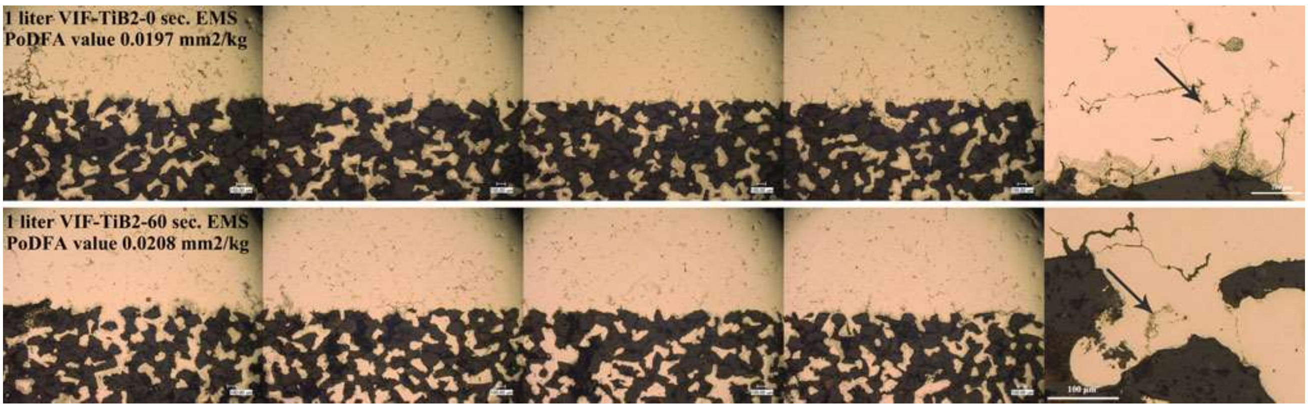

Fig. 8 Micrographs of PoDFA filter (cake) from melt after 0 and 60 s electromagnetically stirring (EMS). Arrows marked TiB_2 particles. Quantitative analytical results insert in upper-left. Results from trial Nr. 9 and 12 conducted in 1 L vacuum induction furnace (VIF)

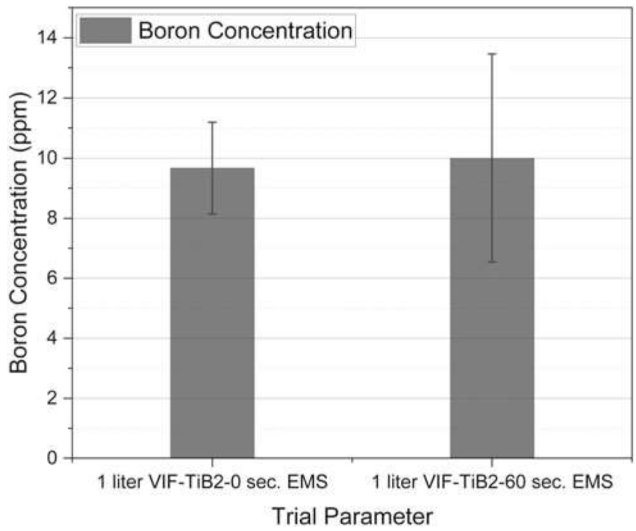

Fig. 9 Spark spectrometer analysis from samples taken from the melt after 0 and 60 s electromagnetic stirring (EMS). Results from trial Nr. 9–14 conducted in 1 L vacuum induction furnace (VIF)

any separation or significant agglomeration of TiB_2 particles after 60 s stirring time. PoDFA metallographic result shown in Fig. 8 also suggests insignificant difference in the collected TiB_2 particles. Nevertheless, in our study the melt was cleaned before charging TiB_2 particles, so most TiB_2 particles were in fact not collected by PoDFA filtration. Therefore we resorted to spark spectrometer analysis for determining TiB_2 concentration in the melt right before PoDFA filtration. The result is given in Fig. 9, which suggests an insignificant variation of TiB_2 concentration in the melt irrespective of melt stirring or not. Such result is in line with time-weight filtration curve and PoDFA results.

Analytical Modelling and Discussions

Reference Materials and Agglomeration

The fabricated A356-SiC and 5xxx-$MgAl_2O_4$ reference materials in fact offer already good basis for agglomeration studies. However no experimental evidence of agglomeration for either types of particles were found. For clarifying the reasons, we tried to examine the kinetics factor, i.e., collision constant. The derivation starts from calculation of magnetic flux density in the center line of the virtual melt [12]:

$$B_0 = k_s k_N \frac{\mu_0 \mu_r N_c I_c}{l_c} \quad (1)$$

where k_s is the shielding factor of the crucible, k_N is the Nagaoka short-coil factor, μ_0 is permeability of free space, μ_r is the relative magnetic permeability of the inductor, N_c is number of inductor turns, I_c is the current, l_c is the length of the coil. With obtained B_0 value, Alfven's velocity u_A can be calculated. Alfven's velocity can be seen as an indicative value of the characteristic melt velocity in an electromagnetically driven melt [13]:

$$u_A = \frac{B_0}{(\mu_0 \mu_r \rho_f)^{0.5}} \quad (2)$$

where ρ_f is the melt density. With the obtained value of u_A, the dissipation rate of turbulent kinetic energy (TKE) ε can be estimated based on following equation [14]:

$$\varepsilon = \frac{u_A^3}{L} \quad (3)$$

where L is the characteristic length of the melt. According to the classic Saffman–Turner collision theory [15], the collision constant C_t can be calculated by:

$$C_t = \sqrt{\frac{8\pi}{3}} d^3 \sqrt{\frac{\varepsilon}{5\nu}} \quad (4)$$

where d is the diameter of the particle, ν is the kinematic viscosity of the melt. Assuming that each collision leads to a decrease of a unit number of particle. One may write down [3]:

$$\frac{dn}{dt} = -C_t n^2 \quad (5)$$

where dn/dt is the particle number density decrease rate, integration of Eq. (5) leads to:

$$\frac{n}{n_0} = \frac{1}{1 + C_t t n_0} \quad (6)$$

where n/n_0 is the remaining particle number density, t is the EMS time of the melt, n_0 is the initial particle number density.

If we input the initial particle concentration 0.1 vol% and treatment time 60 s, the remains particle number density ratio after melt stirring can be calculated. Results are given in Table 3. It can be seen that the particle number density remains as only 0.65% with our input values. As a consequence the average particle size shall be 5 times larger than the reference materials, which was, however, not observed in any of the 0.1 L VIF trials.

Based on established analytical model, insufficient collision rate of the particles can be excluded as a reason for the particle to not form agglomerates. To account for the non-agglomeration character, other factors such as weak adhesion or swift separation of particles towards the near-wall region of the melt shall be considered.

It is worth mentioning that one should be cautious to extrapolate the non-agglomeration indication to all kinds of

Table 3 Estimated fluid and particle dynamic properties

Crucible shielding factor	Nagaoka shielding factor	Magnetic perm.	Melt density	Chara. length	Melt kinematic viscosity	Alfven's velocity	Diss. rate TKE	Particle density remains
/	/	(H/m)	kg/m^3	m	m^2/s	m/s	m^2/s^3	%
k_s	k_N	$\mu_0 * \mu_r$	ρ_f	L	ν	u_A	ε	n/n_0
0.34	0.78	1.26E-06	2445	0.02	4.91E-07	0.2	0.51	0.65

$MgAl_2O_4$ inclusions. In practical situations, $MgAl_2O_4$ inclusions may adopt different morphologies and sizes (e.g., oxide film). Hence their agglomeration behavior (incl. kinetic factor) may deviate from the one we observed in this study.

Size-Dependent Particle Separation

In an electromagnetically driven flow, non-conductive spherical particles are subject to an electromagnetic force f_{EM} whose density is proportional to Lorentz force density F_{EM} [8]:

$$f_{EM} = 0.75 * F_{EM} \tag{7}$$

The force calculated by Eq. (7) will induce a relative velocity of particles in the radial direction which is responsible for the separation of particles. In creep flow ($Re_p < 1$) conditions, the formula of reference radial velocity u_t can be calculated analogously to that of settling velocity [16]:

$$u_t = \frac{1.5 d^2 f_{EM}}{36 \mu_f} \tag{8}$$

where μ_f is melt viscosity. Eq. (8) gives the first criterion for comparing the separation rate of different sized particles. With the increase of particle diameter, the reference radial velocity also increases.

On the other hand, particles present in the melt tend to follow the streamline because of the drag force whose density F_D is given as [16]:

$$F_D = \frac{18\mu_f}{d^2}\left(u_p - u_f\right) \tag{9}$$

where $u_p - u_f$ is the relative velocity of the spherical particle with respect to melt local velocity. Drag force is responsible for carrying out the mixing of particles and hence counteract the localized enrichment of particles in the melt. Under the same flow conditions, particle relaxation time τ_p justifies the faithfulness of the particles to follow streamlines of the flow and hence the tendency of particle to be well-dispersed. The relaxation time τ_p can be calculated by dividing the relative velocity $u_p - u_f$ with particle acceleration, the latter of which can be readily calculated using F_D given in Eq. (9) [17]:

$$\tau_p = \frac{\left(u_p - u_f\right)}{\frac{F_D}{\rho_p}} = \frac{\rho_p d^2}{18\mu_f} \tag{10}$$

In the recirculated electromagnetically driven flow, if a particle has a high value of relation time of a particle, it is more prone to deviate from the streamline of the flow pattern. Equation (10) offers the second criterion for comparing the separation rate of different sized particles.

A combination of Eq. (8) and Eq. (10) makes it possible to compare the separation rate of different sized particles under same flow conditions. For instance, in the 1 L vacuum induction furnace scenario, SiC particles will be separated faster towards the wall region than TiB_2 particles since they have a higher radial terminal velocity and meanwhile they are inclined to fall out of streamlines.

Based on Eq. (8) and Eq. (10), a comparison of particle separation probability of TiB_2, SiC and $MgAl_2O_4$ is schematically drawn in Fig. 10. Note that the spherical particle shape is assumed during the derivation of the models. For other shapes of inclusions, e.g., oxide film, model adaption is necessary to give the right prediction of separation probability.

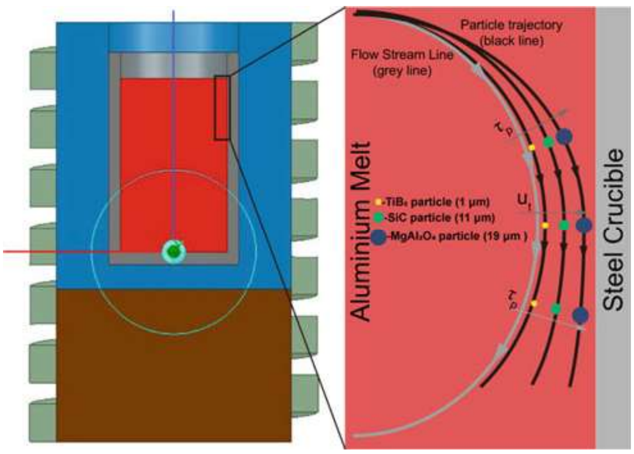

Fig. 10 Schematic of particle separation probability of TiB_2, SiC, and $MgAl_2O_4$ under same flow condition. Density difference has been accounted for

Conclusions

Agglomeration and separation behaviors of non-metallic inclusions in 5xxx alloy melt were investigated in electromagnetically driven flow. The findings are summarized as follows:

- A combination of stir-casting and ultrasound melt treatment is capable of fabricating 5xxx-$MgAl_2O_4$ materials with well dispersed particles.
- No apparent evidence was found for agglomeration tendency of SiC, $MgAl_2O_4$, and TiB_2 particles with respect to their respective as-charged states. Although established analytical model indicates sufficient collision rate provided by the flow.
- Experimental results demonstrate that particle separation rate is positively related to size. Two separation criteria were proposed to explain size-dependent particle separation rate.

Acknowledgements The research leading to these results was carried out in “Project 4 Continuation (P4C)” within Advanced Metals and Process (AMAP) Research Cluster at RWTH Aachen University, Germany. The authors are thankful for the financial support received from P4C members namely: Constellium, Magma, Nemak, Novelis, Speira, Trimet, and Vesuvius. Special thanks addressed to China Scholarship Council (CSC) for the financial support of Cong Li.

References

1. Li C, Li J, Mao Y, Ji J (2017) Mechanism to Remove Oxide Inclusions from Molten Aluminum by Solid Fluxes Refining Method. China Foundry 14(4):233–243
2. Grandfield J (2017) Developments in Inclusion Removal Technology. Light Metals 2017:1429–1434
3. Szekely AG. The Removal of Solid Particles from Molten Aluminum in the Spinning Nozzle Inert Flotation Process. Metall Mater Trans B 7(2):259–270
4. Tian C, Irons GA, Wilkinson DS (1998) Monte Carlo Simulation of Clustering of Alumina Particles in Turbulent Liquid Aluminum. Metall Mater Trans B 29(4):785–791
5. Johansen ST, Taniguchi S (1998) Prediction of Agglomeration and Break-Up of Inclusions during Metal Refining. Light Metals 1998:855–861
6. Marechal L, EI-Kaddah N, Menet P-Y (1993) Influence of Convection on Agglomeration and Removal of Non-Metallic Inclusions in Molten Aluminum. Light Metals 1993:907–913
7. Zhang L, Wang S, Dong A, Gao J, Damoah L. N. W. (2014) Application of Electromagnetic (EM) Separation Technology to Metal Refining Processes: A Review. Metall Mater Trans B 45(6):2153–2185
8. Leenov D, Kolin A (1954) Theory of Electromagnetophoresis. I. Magnetohydrodynamic Forces Experienced by Spherical and Symmetrically Oriented Cylindrical Particles. J Chem Phys 22 (4):683–688
9. Takahashi K and Taniguchi S (2003) Electromagnetic Separation of Nonmetallic Inclusion from Liquid Metal by Imposition of High Frequency Magnetic Field. ISIJ Int 43(6):820–827
10. Ščepanskis M, Jakovičs A, Baake E, Nacke B (2014) Solid Inclusions in an Electromagnetically Induced Recirculated Turbulent Flow: Simulation and Experiment. Int J Multiph Flow 64:19–27
11. Shu D, Sun B, Li K, Li T, Xu Z, Zhou Y (2002) Continuous Separation of Non-Metallic Inclusions from Aluminum Melt Using Alternating Magnetic Field. Mater Lett 55(5):322–326
12. Kennedy MW, Bakken JA and Aune RE (2015) Impact of Coil Geometry on Magnetohydrodynamic Flow in Liquid Aluminium and Its Relevance to Inclusion Separation by Electromagnetophoresis. J Manuf Sci Prod 15(1):69–78
13. Taberlet E and Fautrelle Y (1985) Turbulent Stirring in an Experimental Induction Furnace. J Fluid Mech 159:409–431
14. Kirpo M (2008) Modeling of Turbulence Properties and Particle Transport in Recirculated Flows. Ph.D. thesis, UNIVERSITY OF LATVIA
15. Saffman PG, Turner JS (1956) On the Collision of Drops in Turbulent Clouds. J Fluid Mech 1(1):16–30
16. Gökelma M, Einarsrud KE, Tranell G, Friedrich B (2020) Shape Factor Effect on Inclusion Sedimentation in Aluminum Melts. Metall Mater Trans B 51(2):850–860
17. Guha A (2008) Transport and Deposition of Particles in Turbulent and Laminar Flow. Annu Rev Fluid Mech 40:311–341